RSC Advances

PAPER

View Article Online
View Journal | View Issue

Cite this: *RSC Adv.*, 2025, **15**, 10215

Analysis of hydration, material properties, and pore structure of polymers enhanced with dendritic fibrous nanosilica as a concrete additive

Mohammad Azizi,[a] Amin Honarbakhsh,[*ab] Seyed Mojtaba Movahedifar,[ab] Mehdi Nobahari[ab] and Rahele Zhiani[bcd]

Different cement-based grouting and repair materials have been created and are commonly employed in construction renovation projects. Nevertheless, conventional cement mortars face challenges like limited corrosion resistance and weak bonding strength. Polymers, commonly used as modifiers for repair mortars, provide enhanced mechanical properties, increased resistance to corrosion, and better bonding. Despite these advantages, many polymer modifiers are inherently limited in preventing crack initiation and propagation, while also increasing costs. This study incorporated different amounts of three types of polymers supported on dendritic fibrous nanosilica (DFNS-polymers) into cement mortar to evaluate their effects on mortar performance, pore structure, and cement hydration. The addition of DFNS-polymers significantly improved the durability and workability of the mortar. Moreover, the pore structure was optimized, resulting in a more balanced pore distribution and a reduction in pore and porosity size. This research introduces an effective approach to enhancing the performance of repair mortars by combining polymers with suitable fillers.

Received 11th February 2025
Accepted 26th March 2025

DOI: 10.1039/d5ra00985e

rsc.li/rsc-advances

Introduction

Cement is extensively utilized in global construction and engineering; however, its significant energy consumption and carbon emissions pose environmental concerns.[1–6] In response, the international community is advocating for a low-carbon economy centered on green production and resource recycling.[7–10] This shift has increased the demand for sustainable materials with lower energy use and emissions.[11] Geopolymer materials have emerged as promising alternatives to Portland cement, offering both environmental benefits and superior performance.[12] When combined with solid waste and admixtures, geopolymers can achieve bonding effects comparable to traditional cement while exhibiting enhanced mechanical strength and durability, expanding their application potential.[13]

Various polymers, including polyvinyl alcohol, copolymers, and polystyrene, have been integrated into concrete or mortar mixtures. Epoxy resin is particularly notable for its inherent strength, chemical resistance, superior workability, and water resistance.[14–17] Sun *et al.* demonstrated that incorporating epoxy resin into cement mortar significantly increased tensile strength at optimal epoxy content, while the free water content and elastic modulus decreased linearly.[18–22] More recently, Huseien *et al.* utilized epoxy resin in self-healing cement mortars, finding that adding 10% epoxy improved mechanical properties, with damage recovery and healing efficiency depending on both cracking age and healing duration.[23–26] However, much of the existing research focuses on the relationship between mechanical performance and epoxy content, often overlooking its effect on cement hydration. Additionally, epoxy's high cost and inherent brittleness limit its resistance to crack propagation and initiation, creating a need for epoxy modifications tailored to repair cement mortars.[27–29]

In this research, silica nanoparticles were chemically functionalized with layers of APTPOSS, hyperbranched polyglycerol (HPG), and ionic liquid (IL)-linked microporous conjugated polymers. The covalent bonding between DFNS and APTPOSS, IL, and HPG ensured the stability of the grafted microporous polymers, preventing desorption and eliminating the need for adsorption–desorption equilibrium in DFNS-APTPOSS, DFNS-HPG, and DFNS-IL systems. Unlike physical adsorption methods, these materials were linked through robust chemical bonds. Notably, this is the first documented instance of affixing microporous conjugated polymers onto DFNS surfaces for concrete fabrication. The resulting DFNS-APTPOSS, DFNS-HPG, and DFNS-IL particles exhibited self-dispersing capabilities,

[a]*Department of Civil Engineering, Neyshabur Branch, Islamic Azad University, Neyshabur, Iran. E-mail: amin_honarbakhsh@yahoo.com*

[b]*New Materials Technology and Processing Research Center, Department of Civil Engineering, Islamic Azad University, Neyshabur Branch, Neyshabur, Iran*

[c]*Advanced Research Center for Chemistry, Biochemistry and Nanomaterial, Islamic Azad University, Neyshabur Branch, Neyshabur, Iran*

[d]*Department of Chemistry, Islamic Azad University, Neyshabur Branch, Neyshabur, Iran*

removing the necessity for polycarboxylates to ensure even distribution in cement mixtures. This innovation simplifies the manufacturing process of ultra-high-performance concretes, resulting in materials with enhanced malleability and exceptional mechanical strength. These findings highlight the significant potential of DFNS in advancing the field of performance concrete production.

Experimental section

Preparation of ClPOSS nanoparticles

A mixture of 450 mL of ethanol, 18.2 mL of concentrated hydrochloric acid, and 3-chloropropyltrimethoxysilane (8 g) was stirred at room temperature for 2 weeks. The resulting colorless crystals were collected, and dried under vacuum at 75 °C for 31 h.[28]

Generation of DFNS

A total of 2.3 mL of tetraethoxysilane was added to a mixture consisting of pentanol (6.4 mL) and cyclohexane (19 mL). Subsequently, an aqueous solution containing cetylpyridinium bromide (CPB) and urea was introduced into the blend. The resulting solution was transferred to a reactor and maintained at 88 °C for 3.4 hours. To synthesize the desired material, the DFNS was subjected to a thermal treatment in air at 390 °C for 2.6 hours.

Preparation of APTPOSS

A reaction vessel under a nitrogen atmosphere was charged with ClPOSS (1.7 mmol) and 3-aminopropyltriethoxysilane (13 mmol). The reaction mixture was stirred at 130 °C for a duration of 3.5 days. Afterward, the mixture was filtered, cooled, and washed with acetone and methanol.[29]

Preparation of DFNS-APTPOSS nanoparticles

DFNS (2 mmol) were combined with THF (20 mL) in a beaker, followed by the dispersion of NaH (16 mmol) into the mixture using ultrasonication. 1.1 g of APTPOSS was then introduced at room temperature, and the solution was stirred for an additional 16 hours at 84 °C. The resulting products were collected, sequentially washed with deionized water and methanol, and dried at 110 °C for 3.4 h.

Preparation of DFNS-HPG nanoparticles

DFNS (1.6 mmol) were suspended in a solution composed of 2.3 mmol of CH_3OK and 54 mL of toluene, to which 85 mL of anhydrous dioxane was subsequently added. A total of 3.4 g of glycidol was slowly introduced dropwise over the course of 1 hour. The mixture was then vigorously stirred for an additional 2 hours.

Preparation of DFNS-IL nanoparticles

DFNS (2 mmol) were combined with 18 mL of THF in a beaker, followed by the dispersion of NaH (20 mmol) into the mixture using ultrasonication. Subsequently, 1,3-bis(trimethoxysilylpropyl)imidazolium iodide (16 mmol) was added at r.t., and the solution was stirred for 16 hours at 78 °C. The resulting products were collected, sequentially washed with deionized water and methanol, and dried 130 °C for 3.4 hours.

Common method for the synthesis of concrete

DFNS-polymer was combined with 140 g of deionized water and stirred for 52 minutes. Concurrently, 950 g of standard sand and 280 g of Ordinary Portland Cement were added to the mixer. These dry materials were then amalgamated at a slow speed for 2 minutes. Following this, the previously prepared suspension was added to the mixer within a span of 40 seconds, and an additional 140 g of deionized water was introduced. The amalgam was then stirred at a low velocity for 60 seconds and at a faster pace for an additional 45 seconds. The thoroughly mixed fresh mortar was then poured into cube molds measuring 50 × 50 × 50 mm. These molds were placed on a vibrated until and vibration table no more bubbles surfaced on the mortar. After 24 hours of initial curing, the mortar specimens are demolded and moved to a controlled curing environment for further conditioning. This method ensures the effective incorporation of DFNS-polymer into the concrete mortar.

Substances and methods

The primary materials used to create the fine concrete blends included distilled water, Portland cement, standard fine sand, a protein-based foaming agent, and DFNS-polymer. The Portland cement met the BS12 standard and had a specific gravity of 3.24 with a surface area of 3301 $cm^2\ g^{-1}$. Details of its composition and properties are listed in Tables 1 and 2. Fine sand,

Table 1 Properties of the protein-based foaming agent

Factors	Features
Alkali content	<4.66%
Appearance	Pale brown
Congestion (g cm^{-3})	0.98 ± 0.08 kg L^{-1}
Molar mass	236 g mol^{-1}
Dilution ratio	1 : 28
Chloride content	<0.12%
Specific gravity	1.04
pH	6.0 ± 0.8

Table 2 Chemical constituents of OPC

Substance	LOI	CaO	Al_2O_3	SiO_2	Fe_2O_3	Na_2O	MgO	SO_3	K_2O
Percentage (%)	4.23	18.34	8.12	52.25	2.82	0.36	8.94	4.02	0.89

Table 3 Physical properties of ordinary portland cement (OPC)

Characteristics	Percentage (%)
Specific gravity	3.02
Particularexterior zone ($cm^2\ g^{-1}$)	3301
Setting time (initial/final)	169/804
Compressive strength after 28 days (MPa)	52.1

with particle sizes ranging from 0.21 to 2.29 mm and a specific gravity of 3.02 g cm^{-3}, was employed in accordance with BS12620 standards. Table 3 provides the specifications of the protein-based foaming agent, which had a density of 0.98 kg L^{-1}, per the supplier's data. This foaming agent was chosen for its ability to produce small, isolated, spherical air bubbles. Magnetite nanoparticles with a size range of 60–80 nm and a purity above 98.4% were used in the study.

Results and discussion

The DFNS-HPG, DFNS-IL, and DFNS-APTPOSS were produced using a straightforward 3 step method. DFNS was produced through the condensation of simultaneous hydrolysis and TMOS. Subsequently, the DFNS was equipped with numerous Si–OH groups on their surfaces, which facilitated the functionalization of the DFNS with APTPOSS, 1,3-bis(trimethoxysilylpropyl)imidazolium iodide, and glycidol to form DFNS-APTPOSS, DFNS-IL, and DFNS-HPG (Scheme 1). The optimal combination of the structures HPG, IL, and APTPOSS were explored to ensure the nanostructures remained within the DFNS framework. These nanostructures were subsequently analyzed using various characterization techniques, including FTIR, TGA, TEM, and SEM.

FT-IR analysis was employed to examine the surface modifications of the DFNS-polymer. The DFNS displayed Si–O–Si asymmetric and symmetric stretching vibrations at 806 and 1112 cm^{-1}, along with an H–O stretching vibration at 3398 cm^{-1} (Fig. 1a). The successful grafting of the APTPOSS-based inorganic–organic hybrid onto the DFNS was verified by the presence of two broad peaks 994–1136 cm^{-1}, corresponding to O–Si stretching vibrations. Fig. 1b shows H–C stretching at 2924 cm^{-1} and H–C bending near 1441 cm^{-1}. Peaks at 3117 and 2904 cm^{-1} were assigned to the H–C stretching vibrations of aliphatic and aromatic groups. Additionally, the peaks at 1571 cm^{-1} and 1694 cm^{-1} are associated with the N=C and C=C stretching vibrations of the imidazolium ring (Fig. 1d). These results verify the successful incorporation of the imidazolium IL onto the DFNS surface.

The structures of the synthesized DFNS, DFNS-APTPOSS, DFNS-HPG, and DFNS-IL were examined using TEM and SEM. The DFNS microspheres exhibited a uniformity, monodispersity, and fibrous structure, with an average diameter ranging from 350 to 380 nm. The TEM image in Fig. 2 further reveals that the distance between two fibers was about 14–18 nm. After the incorporation of APTPOSS, HPG, and IL, the fibers became distinctly identifiable due to differences in their contrast (Fig. 2). The as-prepared nanoparticles maintained their fibrous shape without significant aggregation. Fig. 3 illustrates the thermal behavior of DFNS, DFNS-APTPOSS, DFNS-HPG, and DFNS-IL. The weight loss observed below 130 °C was attributed to the removal of chemisorbed and physisorbed solvents from the surface of the DFNS-polymers nanomaterial. In the second stage (130–550 °C), the weight loss ranged from 20–35 wt% for all the catalysts, which is associated with the degradation of organic group derivatives.

The N2 adsorption–desorption isotherms of DFNS, DFNS-APTPOSS, DFNS-HPG, and DFNS-IL displayed a typical type IV curve, aligning with documented findings on conventional fibrous silica spheres (Fig. 4). The BET surface areas for DFNS, DFNS-APTPOSS, DFNS-HPG, and DFNS-IL were 489, 307, 361, and 392 $m^2\ g^{-1}$. The pore diameters were 14.02, 9.72, 10.43, and

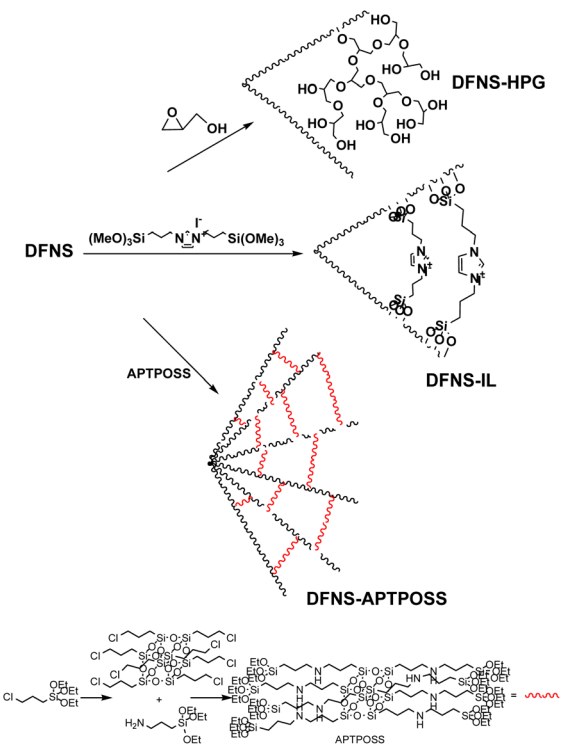

Scheme 1 Schematic representation of the DFNS-polymer synthesis process.

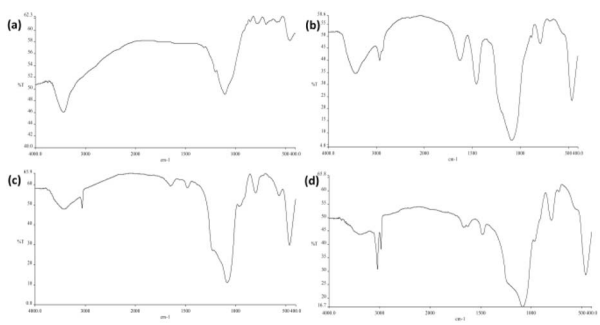

Fig. 1 FTIR spectra of (a) DFNS, (b) DFNS-APTPOSS, (c) DFNS-HPG, and (d) DFNS-IL.

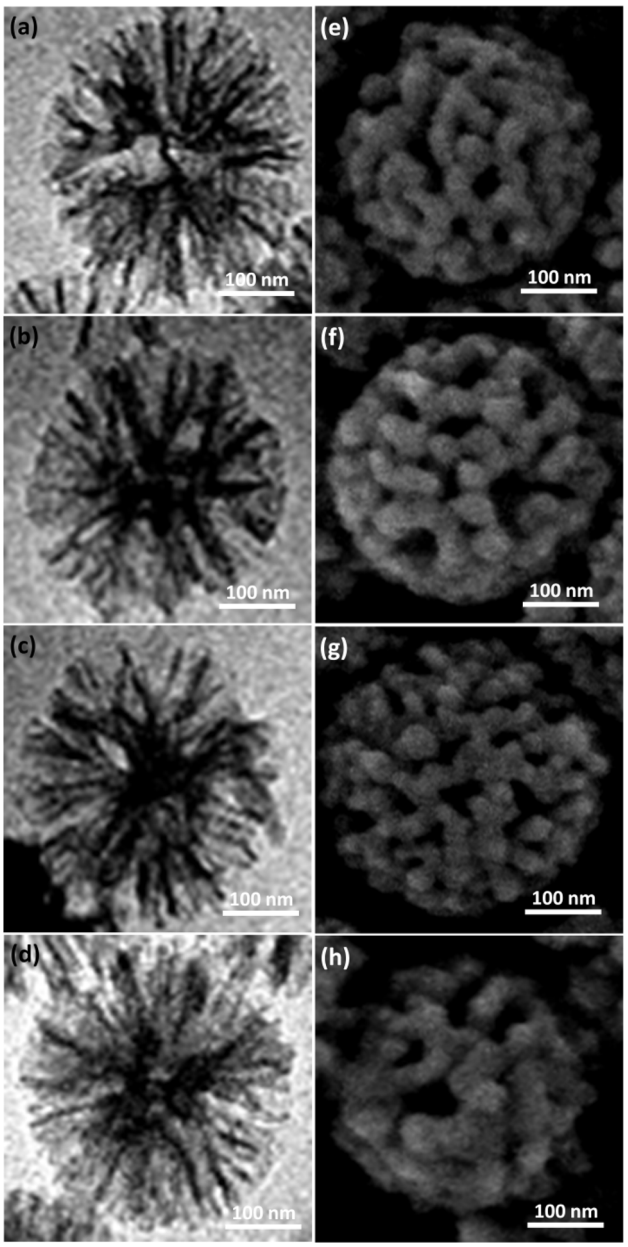

Fig. 2 TEM images of DFNS (a), DFNS-APTPOSS (b), DFNS-HPG (c), and DFNS-IL (d); SEM images of DFNS (e), DFNS-APTPOSS (f), DFNS-HPG (g), and DFNS-IL (h).

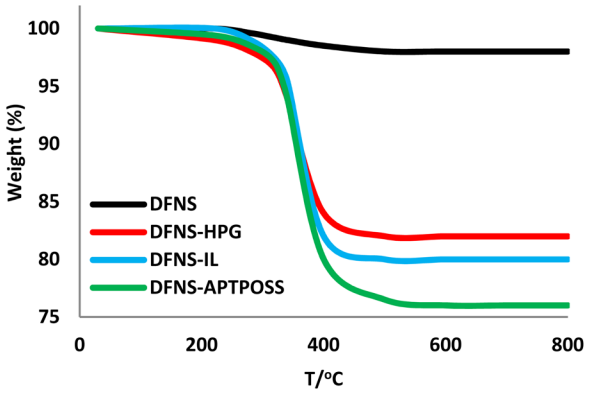

Fig. 3 TGA diagram of DFNS, DFNS-APTPOSS, DFNS-HPG, and DFNS-IL.

11.64 nm, and the pore volumes were 1.67, 1.24, 1.31, and 1.46 $cm^3\ g^{-1}$. The nitrogen sorption analysis of DFNS-APTPOSS, DFNS-HPG, and DFNS-IL confirmed a uniform and regular mesostructure, with a decrease in pore diameter, pore volume, and surface area compared to the DFNS (Table 4). Functionalization with Si–X (X = IL, HPG, and APTPOSS) led to a notable decrease in pore volumes, likely caused by the increased loading of the sensing probe, which occupies a substantial portion of the silica spheres' internal volume.

The hydration behavior of cement pastes incorporating different DFNS-polymer contents was tracked over 5 days using an isothermal calorimeter. The heat flow and cumulative heat release curves obtained are shown in Fig. 5a. In comparison to the control samples, which displayed the highest exothermic and the fastest hydration peak, incorporating polymers into the cement progressively reduced the hydration rate and postponed the exothermic peak as the polymer content increased. This behavior can be attributed to the high concentration of DFNS-polymers, which became trapped in the capillary pores and surrounded the surface of cement gel particles, hindering the growth and nucleation of hydration products. Fig. 5b presents the cumulative heat release of the paste specimens over 5 days, showing a positive correlation with curing time and a negative correlation with DFNS-polymer content. As the DFNS-polymer content increased, less heat was generated during cement hydration, leading to a reduced cumulative heat release. Thus, the presence of DFNS-polymers not only slowed the hydration reaction rate but also potentially reduced the overall degree of hydration.

Repair mortar must exhibit excellent workability to ensure efficient application on construction sites. Fig. 6 shows the apparent density and slump of polymer-based cement mortar. As per the Chinese standard JC/T 2381-2016, the slump for repair mortar must be at least 30 mm. As the *p*/*c* ratio grew, the slump also increased (Fig. 6a). The standard requirements were met once the *p*/*c* ratio surpassed 8%. This is due to the aerating effect of DFNS-polymers, which generates numerous tiny air bubbles during the mortar mixing process. These bubbles create a "rolling ball effect" within the mixture, improving its flowability. This slowed down setting of the cement and the hydration, which in turn contributed to an improvement in the mortar's workability. Fig. 6b displays the apparent densities of polymer-based cement mortar. As the DFNS-polymer content increased, the apparent density consistently decreased. Due to the lower density of DFNS-polymers compared to cement slurry, and the increased air content from the introduction of air bubbles during mixing, the apparent density of the polymer-based cement mortar was reduced. A negative correlation exists between apparent density and mortar slump, with both factors enhancing workability. In other words, incorporating DFNS-polymers improved the workability of the repair mortar.

Fig. 7 shows the mechanical properties of polymer-based cement mortar with varying DFNS-polymer contents. The

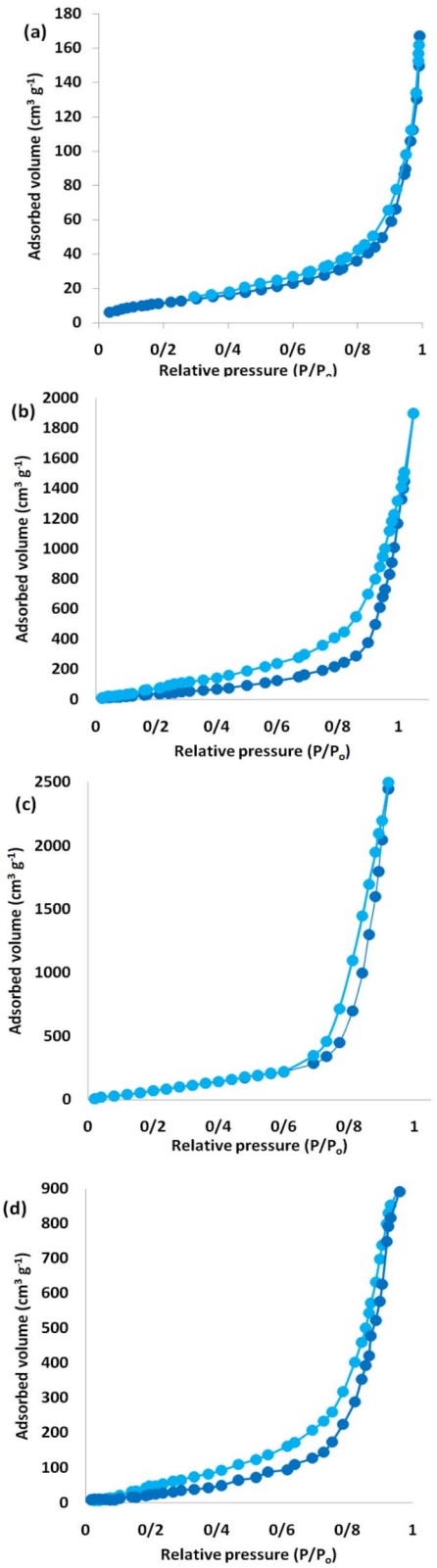

Fig. 4 Adsorption–desorption isotherms of (a) DFNS, (b) DFNS-APTPOSS, (c) DFNS-HPG, and (d) DFNS-IL.

modification with DFNS-polymers had a negative effect on the compressive strength of the mortars cured for 5, 10, and 30 days. At each curing age, the compressive strength of the

Table 4 Structural parameters of nanoparticles were analyzed through nitrogen sorption experiments, providing insights into surface area, pore volume, and pore size characteristics of these materials

Nanoparticles	V_t (cm^3 g^{-1})	S_{BET} (m^2 g^{-1})	D_{BJH} (nm)
DFNS	1.67	489	14.02
DFNS-APTPOSS	1.24	307	9.72
DFNS-HPG	1.31	361	10.43
DFNS-IL	1.46	392	11.64

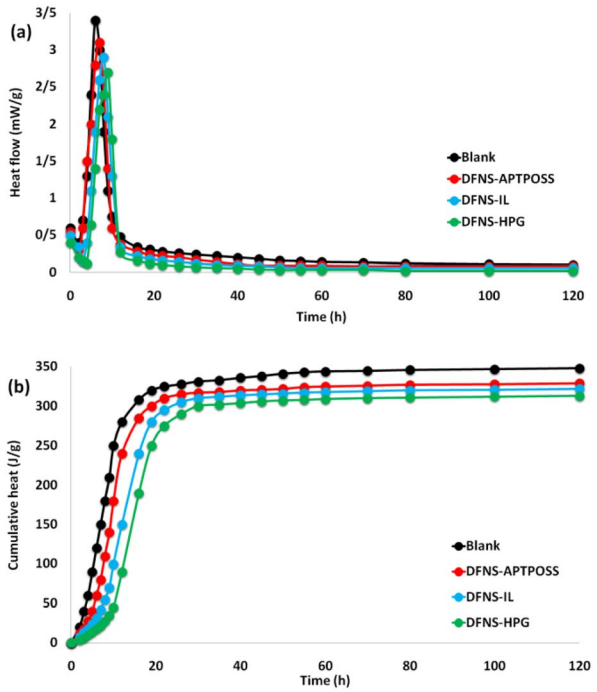

Fig. 5 Heat flow profiles (a) and cumulative heat release profiles (b) of cement pastes incorporating various DFNS-polymers.

mortars tended to decrease as the *p*/*c* ratio increased. This can be attributed to multiple factors: first, the addition of DFNS-polymers slowed the cement hydration process; second, the resins in the mortar needed curing time, and uncured resins were unable to provide sufficient strength; third, the cured DFNS-polymers had a lower elastic modulus compared to the cement hydration products. On the other hand, the ongoing cement hydration produced alkali compounds such as $Ca(OH)_2$, which potentially activated epoxy curing reactions, resulting in a slight enhancement in flexural and compressive strength. After 30 days of curing, the cement mortar with the polymer displayed similar compressive strengths. Given that the curing of DFNS-polymers occurred quickly and was almost finished by 10 days, the strength variation between the 10 days and 30 days specimens was negligible. The influence of DFNS-polymers on the mechanical strength of the mortar at later stages of curing was therefore negligible.

Fig. 8 illustrates the flexural strength of the cement mortar modified with polymer. During the early stages, a higher content of DFNS-polymers resulted in a decrease in the flexural

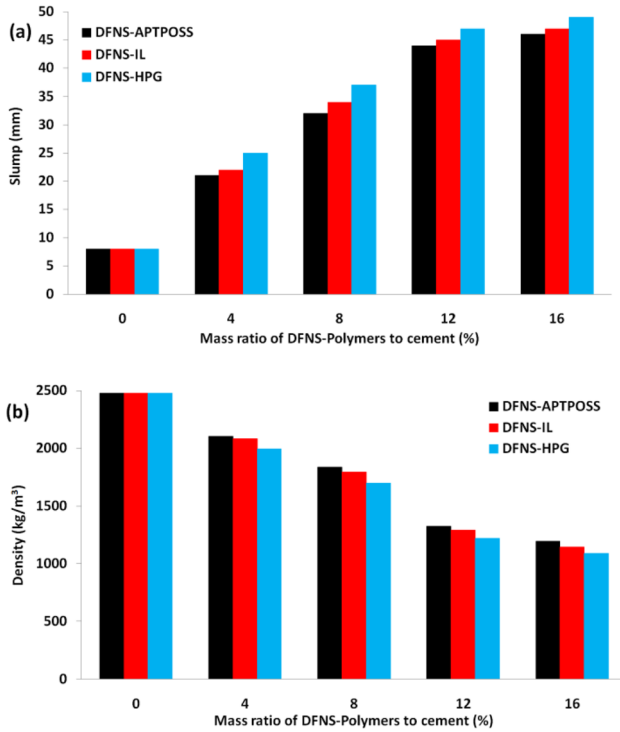

Fig. 6 Slump (a) and apparent densities (b) of cement mortar with polymer based with different DFNS-polymers contents.

strength of the cement mortar. The uncured resins present in the paste slowed down the cement hydration process, leading to a reduction in the material's strength. A reduced polymer-to-cement (p/c) ratio proved beneficial for enhancing the long-term mechanical performance of the polymer-modified cement mortar. After 10 days of curing, a crosslinked polymer network had developed, giving the mortar a flexural strength similar to that of conventional mortars, approximately 8.0–8.6 MPa. The strength gap between the cement mortar with polymer specimens narrowed as curing continued. The mortar with 8% DFNS-HPG exhibited the highest flexural strength after 30 days of curing. However, excess unreacted DFNS-polymers may have been trapped in the system, not contributing to the strength and negatively impacting the flexural strength. As a result, notable reductions in flexural strength were seen in the cement mortar with 10% and 12% DFNS-polymers. Incorporating DFNS-polymers lowered the c/f ratio, reflecting enhanced toughness. This improvement is attributed to the polymer's filling effects, adhesive properties, and the inherent flexibility of DFNS-polymers. Using too little DFNS-polymers can prevent the formation of a cohesive polymer network, while excessive amounts may result in clumping and the creation of an overly dense polymer layer in the mortar (Fig. 9).

The interface flexural strength of the specimens is largely controlled by interfacial forces, such as ionic bonds, covalent bonds, and van der Waals interactions, between the adhesive material and the substrate. Incorporating DFNS-polymers greatly enhanced the flexural strength at the interface of the polymer-modified cement mortar (Fig. 10). As the p/c ratio

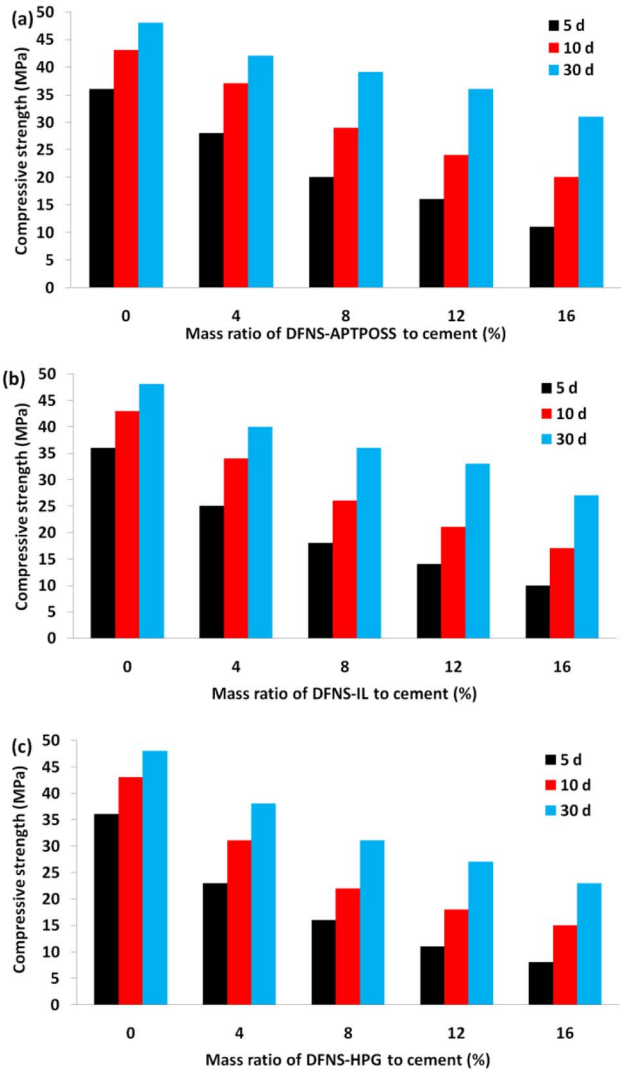

Fig. 7 Compressive strengths of cement mortar with polymer specimens with (a) DFNS-APTPOSS, (b) DFNS-IL, and (c) DFNS-HPG.

increased, the flexural strength at the interface of the polymer-modified cement mortar first improved and eventually leveled off. In comparison to the blank mortar, the cement mortar with 8% DFNS-polymers reached its maximum interface flexural strength after 30 days of curing. The fracture surface of the blank mortar was smooth in appearance, whereas the polymer-modified cement mortar exhibited a rougher surface with residual substrate fragments, indicating stronger bonding strength in the polymer-modified mortar.

The mechanical properties of polymer-modified cement mortar after immersion in 8% Na_2SO_4 and 8% NaCl solutions are shown in Fig. 11. The mechanical properties of all polymer-modified cement mortars initially improved during the early stages of erosion but experienced a notable decline thereafter. The cement mortar with polymers exhibited the highest compressive and flexural strengths after 10 days of immersion. The hydration products of cement play a crucial role in determining the corrosion resistance of repair mortar. The

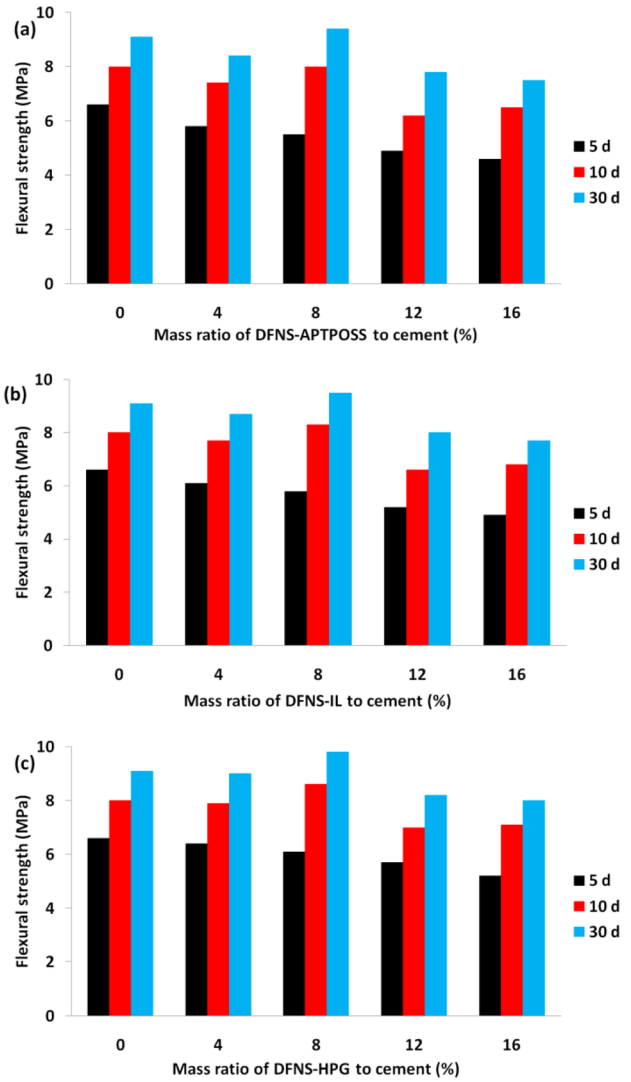

Fig. 8 Flexural strengths of cement mortar with polymer specimens with DFNS-APTPOSS (a), DFNS-IL (b), and DFNS-HPG (c).

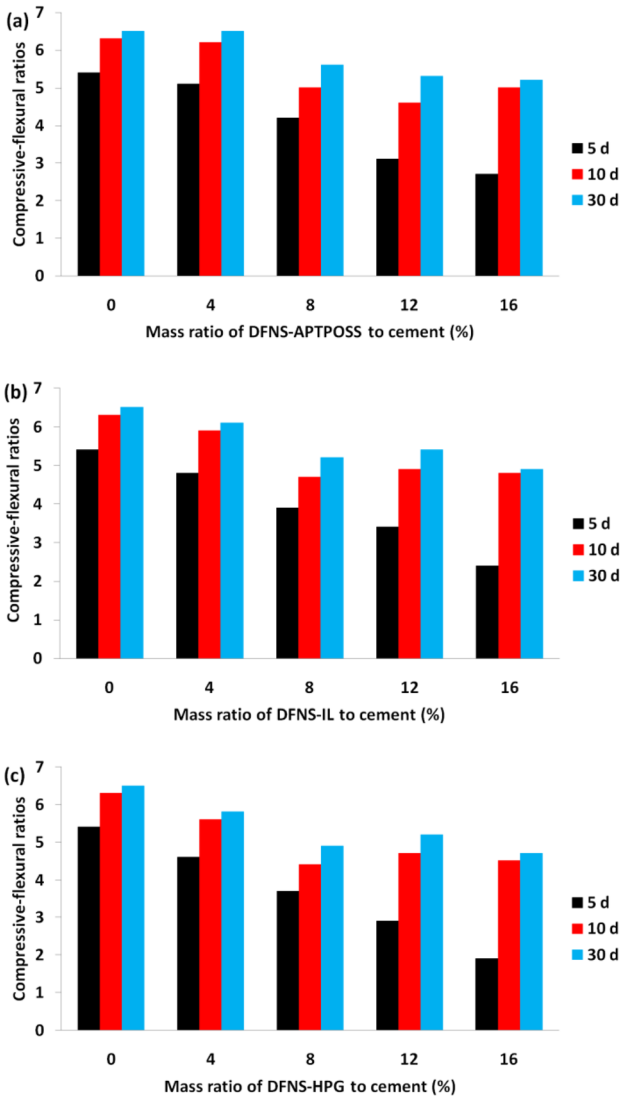

Fig. 9 Compressive-flexural ratios of cement mortar with polymer specimens with DFNS-APTPOSS (a), DFNS-IL (b), and DFNS-HPG (c).

infiltration of chloride and sulfate ions can compromise the mortar's microstructure, leading to strength reduction and structural degradation. Both chloride and sulfate ions can react with dihydrate gypsum, forming ettringite, calcium oxychloride hydrate, and $Ca(OH)_2$. The erosion reaction products have greater volumes compared to $Ca(OH)_2$. During the initial phase of erosion, the mortar structure compacts. As erosion advances, the reaction products grow and exert pressure within the mortar structure. Once the internal pressure from this expansion exceeds a certain threshold, microcracks are formed, leading to the deterioration of the mortar. Remarkably, the inclusion of DFNS-polymers considerably enhanced the corrosion resistance of the polymer-modified cement mortar. The film structure of DFNS-polymers within the mortar effectively fills the pores, blocking the infiltration of corrosive solutions. This minimized the interaction between ions and hydration products, reducing the formation of expansive compounds and enhancing the mortar's corrosion resistance.

Since the pore structure of mortars is greatly influenced by polymer content and filler addition, water absorption serves as a crucial metric for evaluating these structural changes (Fig. 12). However, the incorporation of DFNS-polymers into the mortar generated numerous bubbles during the mixing process, which created additional voids for water retention and resulted in higher water absorption. A high content of DFNS-polymers effectively occupied the pores, reducing water absorption by outperforming the air bubbles in filling the voids.

Micropores in cement-based materials are typically categorized into four groups according to their diameters and influence on mortar strength: highly detrimental pores, detrimental pores, moderately detrimental pores, and non-detrimental pores. As shown in Fig. 13, by incorporating DFNS-polymers, the percentage of harmful pores in the mortar was reduced, while the proportion of harmless pores increased, leading to a more balanced pore structure. Replacing 8% of the standard sand with DFNS-polymers resulted in an improvement in the

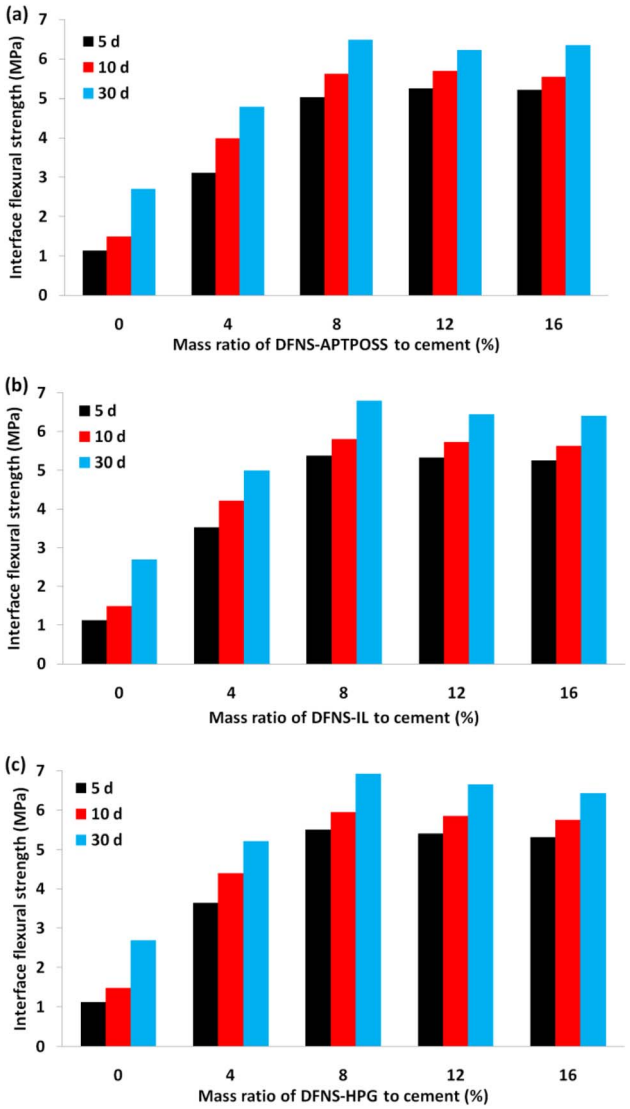

Fig. 10 Interface flexural strengths of cement mortar with polymer specimens with (a) DFNS-APTPOSS, (b) DFNS-IL, and (c) DFNS-HPG.

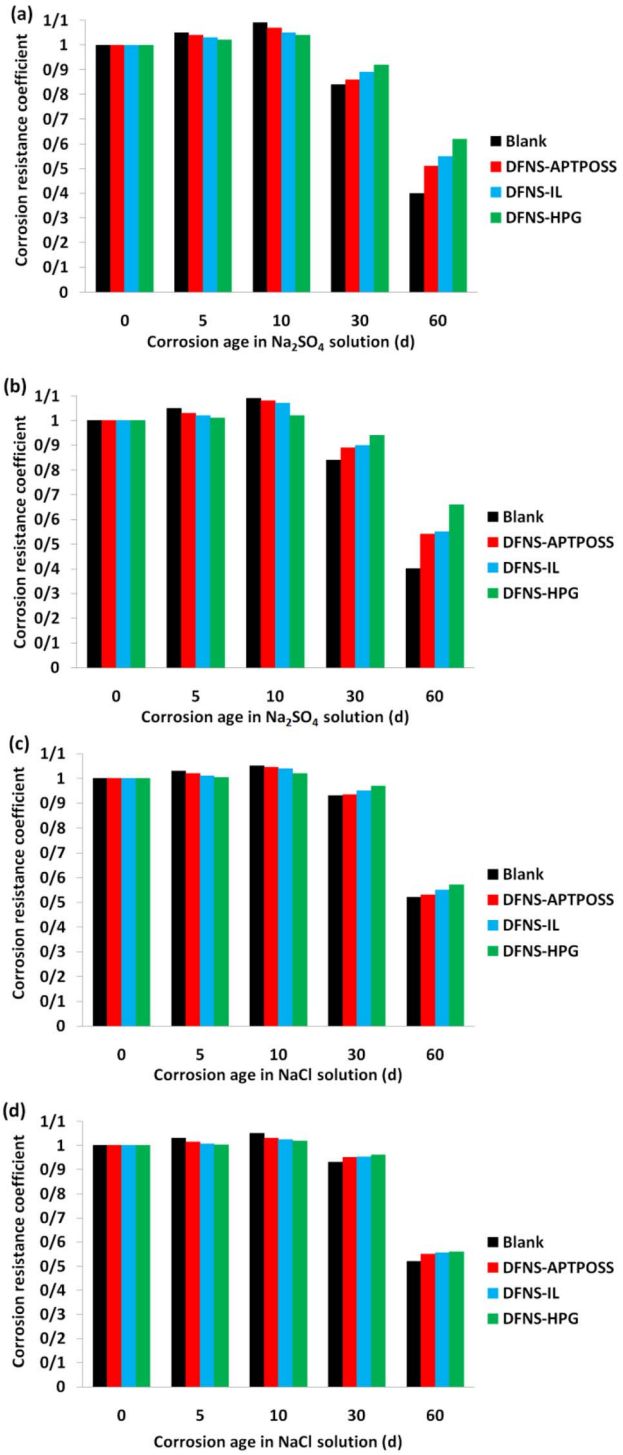

Fig. 11 Corrosion resistance coefficients of cement mortar containing polymers over aging time in an 8% Na_2SO_4 solution, evaluated based on flexural strength (a) and compressive strength (b); corrosion resistance coefficients of cement mortar containing polymers over aging time in an 8% NaCl solution, evaluated based on flexural strength (c) and compressive strength (d).

pore structure and a reduction in the average pore diameter to approximately 18 nm.

Fig. 14 illustrates the impact of different weight ratios of DFNS-polymers on the porosity of concrete. DFNS-polymers demonstrated the lowest porosity, with a reduction of about 25% compared to the control specimen. This decrease is due to the enhanced hydration induced by DFNS-polymers, which improved the material's filling capability. DFNS-APTPOSS, DFNS-IL, and DFNS-HPG exhibited porosities of 40%, 37%, and 35%, while the control sample exhibited a porosity of 47% on the 10th day. This decrease in porosity can be attributed to the accumulation of DFNS-polymers, which reduced their capacity to fill the voids in the cementitious composite. The presence of DFNS-polymers improved the concrete microstructure by number of voids and reducing the size, the cementitious matrix and enlarging the connection between the filler, and enhancing the concrete's strength. Furthermore, the addition of DFNS-polymers to the concrete resulted in the development of blocked pores, minimizing pore openings and lowering the concrete composite's absorption coefficient.

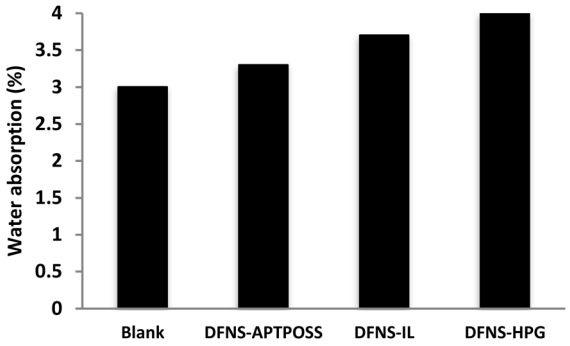

Fig. 12 The water absorption characteristics of the mortar specimens were evaluated based on their pore sizes.

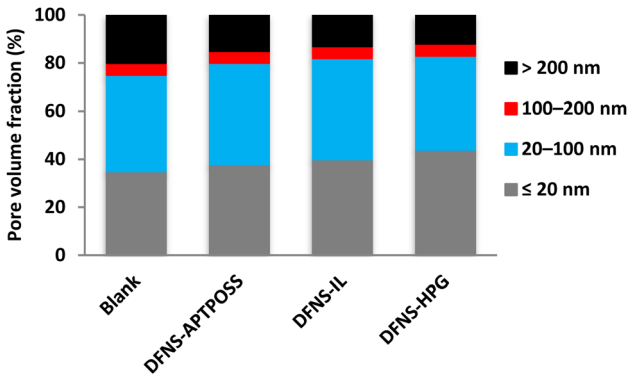

Fig. 13 Pore size distribution of the mortar samples.

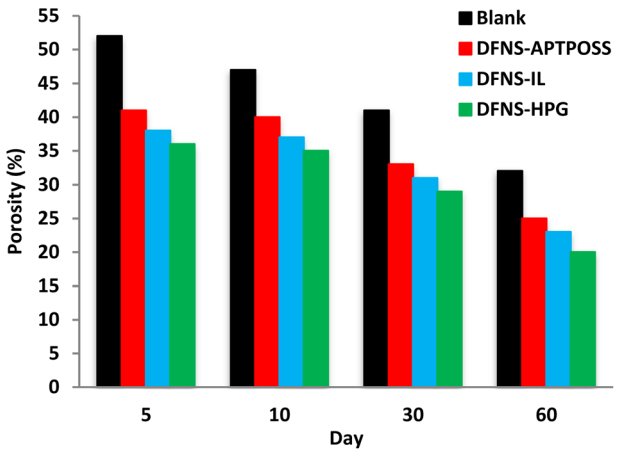

Fig. 14 The impact of different weight fractions on the porosity of concrete.

Concrete drying shrinkage refers to the volume reduction that occurs when moisture is lost from the concrete, causing a decrease in its overall size. This shrinkage is a primary contributor to cracking in concrete. The paste created from DFNS-polymers cement behaves as a viscoelastic material, indicating that the volume reduction results from both viscous and elastic mechanisms. From the data, it is clear that drying

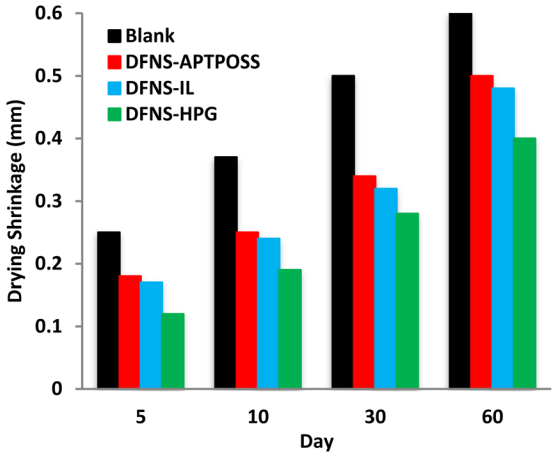

Fig. 15 The effect of different mass fractions on the drying shrinkage of concrete.

shrinkage increases over time for all mixtures (Fig. 15). The control sample exhibited the greatest reduction in moisture content, resulting in the highest shrinkage. However, the incorporation of DFNS-polymers significantly reduced the drying shrinkage. The absorbed energy is then dispersed to the surrounding matrix, which reduces the tensile stress in the concrete, ultimately minimizing the potential for crack formation. When the DFNS-polymers are uniformly distributed throughout the cement paste, the cement's hydration products tend to accumulate around the DFNS-polymers, which act as nucleation sites. This results in a more stable microstructure and improved resistance to drying shrinkage and fracture.

Fig. 16a compares the weight loss between DFNS, DFNS-APTPOSS, DFNS-IL, and DFNS-HPG, highlighting the beneficial effect of DFNS-polymers on frost resistance. The results demonstrate that DFNS-polymers exhibited significantly lower weight loss compared to the DFNS and blank samples, indicating better resistance to frost damage. Concrete specimens incorporating DFNS, DFNS-APTPOSS, DFNS-IL, and DFNS-HPG exhibited enhanced resistance to freeze–thaw cycles compared to samples lacking these nanoparticles. Fig. 16b presents the compressive strength of the concrete samples after exposure to different freeze–thaw cycles. The findings indicate that after 250 freeze–thaw cycles, concrete containing around 1.0% DFNS-polymers experienced the least decline in compressive strength while maintaining the highest overall strength. This indicates that the incorporation of DFNS-polymers significantly enhanced the freeze–thaw durability of the concrete, helping to maintain its strength even after repeated exposure to freezing and thawing conditions.

The acid resistance of concrete was assessed, focusing on its durability in a sulfuric acid (H_2SO_4 5%) environment. Concrete samples incorporating DFNS-polymers exhibited enhanced resistance to sulfate attack, maintaining structural integrity more effectively than control samples. Following 15 weeks of exposure to the acid solution, the concrete samples containing DFNS-polymers experienced the least weight loss, measuring around 1.0%, indicating superior resistance to acid

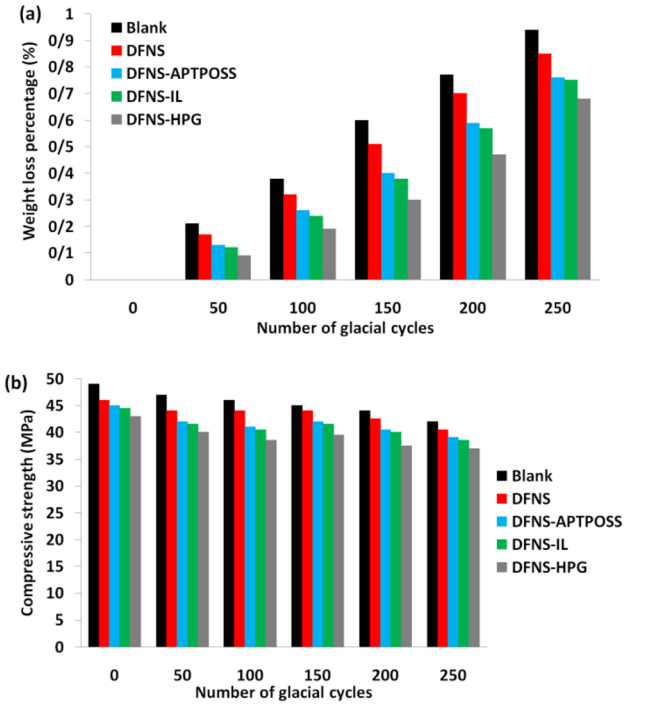

Fig. 16 (a) Weight loss comparison of concrete samples incorporating DFNS, DFNS-APTPOSS, DFNS-IL, and DFNS-HPG after freeze–thaw cycles; (b) compressive strength variations of samples subjected to different freeze-thaw cycles.

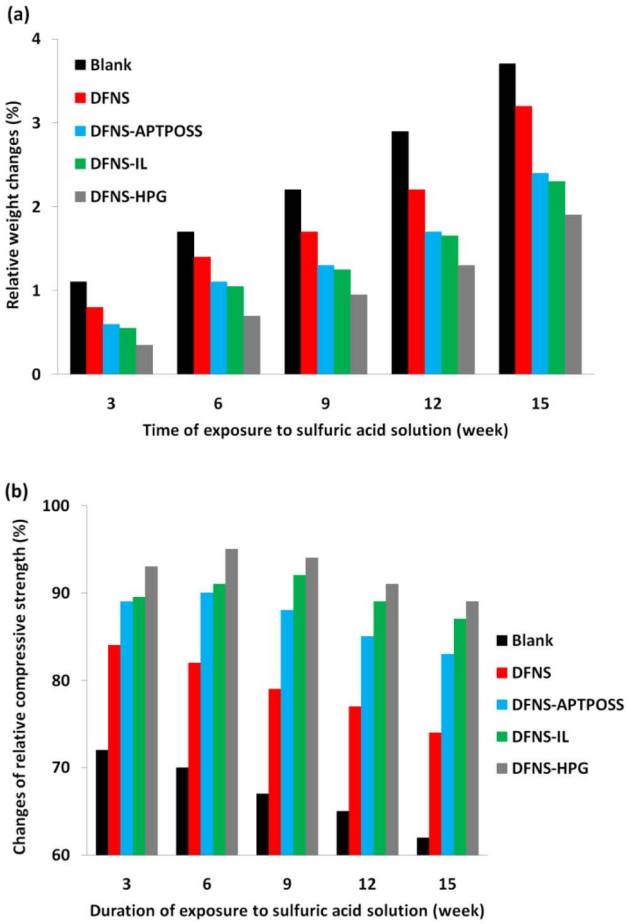

Fig. 17 (a) Relative weight variations and (b) relative compressive strength changes of concrete samples incorporating DFNS-polymers after exposure to sulfuric acid.

deterioration. As shown in Fig. 17a, the control sample experienced the greatest weight loss, while the DFNS sample exhibited higher weight loss than the DFNS-polymers sample. Additionally, a compressive strength assessment was conducted on the concrete samples exposed to H_2SO_4 for 3, 6, 9, 12, and 15 weeks. Fig. 17b presents a comparison of the relative strength of these samples against the control sample. Interestingly, the concrete incorporating DFNS-polymers was the only sample to show an increase in compressive strength after six weeks of exposure. This enhancement was due to the deposition of acid reaction products, which effectively filled the voids in the concrete. By the ninth week, the compressive strength of the DFNS-polymers sample showed an increase, whereas the strength of other samples declined. After 15 weeks, all samples exhibited a more pronounced reduction in compressive strength compared to the DFNS-polymers sample, highlighting its superior resistance to sulfuric acid attack.

As shown in Fig. 18, after curing for 5 to 60 days, the ultrasonic wave velocity in concrete samples containing DFNS-polymers was higher than that in the control concrete. This rise in velocity indicates that DFNS-polymers efficiently occupy the voids within the concrete, facilitating the early-stage development of additional calcium–silicate–hydrate (C–S–H) gel. This process helps reduce the porosity and increase the density of the concrete specimens, allowing ultrasonic waves to travel through the material more quickly. The results of this ultrasonic pulse velocity analysis align with the findings from the compressive and splitting tensile strength tests, further supporting the idea that specimens containing DFNS-polymers exhibit superior performance. This enhancement is mainly attributed to the capability of DFNS-polymers and DFNS to occupy gaps between coarse cement particles, significantly minimizing microscopic voids within the concrete matrix. This enhanced material performance helps improve the overall structural integrity and durability of the concrete.

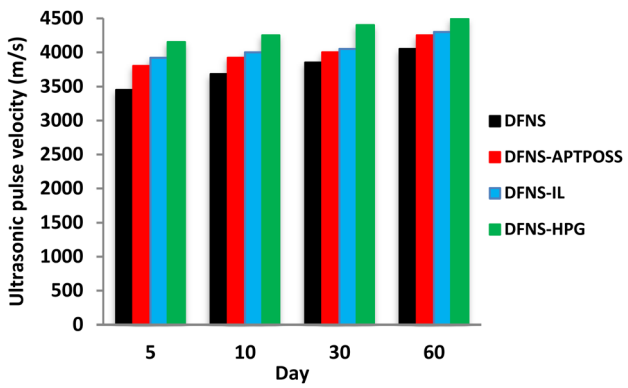

Fig. 18 Ultrasonic test results for different ratios of DFNS and DFNS-polymers at 5, 10, 30, and 60 days.

Conclusions

This study presents a straightforward method for covalently grafting polymers (APTPOSS, IL, and HPG) onto the surface of dendritic fibrous nanosilica, leading to the formation of DFNS-APTPOSS, DFNS-IL, and DFNS-HPG. The influence of these modified DFNS on workability, cement hydration, durability, and mechanical properties was examined, and the preparation method and optimal mix ratio were established. This study provides a strategy to optimize the performance of repair mortar while seamlessly integrating nanotechnology into its practical applications:

- The DFNS-polymers demonstrated a plasticizing effect, as reflected in the decreased energy needed for mixing ultra-high-performance concretes.

- Mortars with DFNS-polymers exhibited higher compressive strength compared to the reference sample. DFNS-polymers exhibited enhanced uniformity in their distribution throughout the cement matrix.

- The covering effect of DFNS-polymers partially restricted the interaction between cement and water, delaying cement hydration and extending the mortar's setting time. This retardation increased with higher DFNS-polymers content. Consequently, the production of hydration products such as H–S–C and $Ca(OH)_2$ decreased, resulting in reduced mortar strength during its early stages.

- Adding polymers to cement pastes improves workability and reduces their density. DFNS-polymers demonstrated superior strength and enhanced resistance to chloride and sulfate ion corrosion compared to conventional repair mortar, achieving optimal results with an 8% polymer-to-cement (p/c) ratio. Both the compressive and flexural strengths met the required standards.

- Overall, the DFNS-polymers were evenly distributed within the mortar, significantly improving its workability and durability. Notably, these DFNS-polymers contributed to a reduction in porosity and water absorption. Proper use of DFNS-polymers enhanced the pore structure by decreasing pore diameters, increasing the proportion of harmless pores and reducing harmful ones.

List of abbreviations

DFNS	Dendritic fibrous nanosilica
APTPOSS	Octakis[3-(3-aminopropyltriethoxysilane)propyl] octasilsesquioxane
HPG	hyperbranched polyglycerol
IL	Ionic liquid
THF	Tetrahydrofuran
OPC	Ordinary portland cement
TEM	Transmission electron microscopy
SEM	Scanning electron microscope
BET	Brunauer–Emmett–Teller
TGA	Thermal gravimetric analysis
FTIR	Fourier transform infrared spectroscopy

Data availability

The data supporting the findings of this study are available within the article.

Conflicts of interest

There are no conflicts to declare.

Notes and references

1 H. Hashim, M. R. Ramlan, L. J. Shiun, H. C. Siong, H. Kamyab, M. Z. Abd Majid and C. T. Lee, *Energy Procedia*, 2015, **75**, 2993–2998.
2 A. Naderipour, Z. Abdul-Malek, R. Naveed Arshad, H. Kamyab, S. Chelliapan, V. Ashokkumar and J. Tavalaei, *Clean Technol. Environ. Policy*, 2021, **23**, 183–201.
3 H. Hashim, M. A. Zubir, H. Kamyab and M. F. Islam Zahran, *Chem. Eng. Trans.*, 2022, **97**, 511–516.
4 H. U. Ahmed, A. S. Mohammed, R. H. Faraj, S. M. A. Qaidi and A. A. Mohammed, *Case Stud. Constr. Mater.*, 2022, **16**, e01036.
5 H. U. Ahmed, A. S. Mohammed, R. H. Faraj, A. A. Abdalla, S. M. A. Qaidi, N. H. Sor and A. A. Mohammed, *Neural Comput. Appl.*, 2023, **35**, 12453–12479.
6 S. A. Ahmad, B. H. Saeed, S. N. Hussein, H. U. Ahmed, S. K. Rafiq, D. A. Ahmad and K. O. Fqi, *J. Build. Pathol. Rehabil.*, 2024, **9**, 29.
7 A. A. Mohammed, H. Nahazanan, N. A. M. Nasir, G. F. Huseien and A. H. Saad, *Materials*, 2023, **16**, 2020.
8 T. M. Mendes, D. Hotza and W. L. Repette, *Rev. Adv. Mater. Sci.*, 2015, **40**, 89–96.
9 F. Sanchez and K. Sobolev, *Constr. Build. Mater.*, 2010, **24**, 2060–2071.
10 A. Folli, C. Pade, T. B. Hansen, T. De Marco and D. E. Macphee, *Cem. Concr. Res.*, 2012, **42**, 539–548.
11 L. P. Singh, S. R. Karade, S. K. Bhattacharyya, M. M. Yousuf and S. Ahalawat, *Constr. Build. Mater.*, 2013, **47**, 1069–1077.
12 R. Goyal, V. K. Verma and N. B. Singh, *Mater. Today: Proc.*, 2022, **65**, 1956–1963.
13 M. Kumar, M. Bansal and R. Garg, *Mater. Today: Proc.*, 2021, **43**, 892–898.
14 Y. K. Jo, *Constr. Build. Mater.*, 2008, **22**, 911–920.
15 L. Li, W. Liu, Q. You, M. Chen and Q. Zeng, *J. Cleaner Prod.*, 2020, **259**, 120853.
16 Z. Zheng, Y. Li, X. Ma, X. Zhu and S. Li, *Constr. Build. Mater.*, 2019, **197**, 319–330.
17 X. Zhang, M. Du, H. Fang, M. Shi, C. Zhang and F. Wang, *Constr. Build. Mater.*, 2021, **299**, 124290.
18 J. Fan, G. Li, S. Deng and Z. Wang, *Appl. Sci.*, 2019, **9**, 2178.
19 Y. Li, X. Liu, J. Yuan and M. Wu, *Constr. Build. Mater.*, 2015, **100**, 122–128.
20 J. P. Moretti, A. Sales, V. A. Quarcioni, D. C. B. Silva, M. C. B. Oliveira, N. S. Pinto and L. W. S. L. Ramos, *J. Cleaner Prod.*, 2018, **187**, 473–484.
21 R. Wang and C. Meyer, *Cem. Concr. Compos.*, 2012, **34**, 975–981.

22 J. Luo, Q. Li, T. Zhao, S. Gao and S. Sun, *Constr. Build. Mater.*, 2013, **49**, 766–771.
23 A. M. Onaizi, G. F. Huseien, N. H. A. S. Lim, M. Amran and M. Samadi, *Constr. Build. Mater.*, 2021, **306**, 124850.
24 G. F. Huseien and K. W. Shah, *Constr. Build. Mater.*, 2020, **235**, 117458.
25 G. F. Huseien, A. R. M. Sam, K. W. Shah, A. M. A. Budiea and J. Mirza, *Constr. Build. Mater.*, 2019, **225**, 132–145.
26 K. W. Shah and G. F. Huseien, *Biomimetics*, 2020, **5**, 47.
27 G. F. Huseien, A. R. M. Sam, I. Faridmehr and M. H. Baghban, *Materials*, 2021, **14**, 1255.
28 K. Murari, R. Siddique and K. K. Jain, *J. Mater. Cycles Waste Manage.*, 2015, **17**, 13–26.
29 X. Zheng, J. Pan, S. Easa, T. Fu, H. Liu, W. Liu and R. Qiu, *J. Build. Eng.*, 2023, **76**, 107246.